



Phenotypic and Genotypic Characteristics of Novel Mouse Cell Line (NIH/3T3)-Adapted Human Enterovirus 71 Strains (EV71:TLLm and EV71:TLLmv)

Carla Bianca Luena Victorio^{1,2}, Yishi Xu^{1,2}, Qimei Ng¹, Vincent T. K. Chow², Kaw Bing Chua^{1*}

¹ Temasek Lifesciences Laboratory, 1 Research Link, National University of Singapore, Singapore, ² Host and Pathogen Interactivity Laboratory, Department of Microbiology, Yong Loo Lin School of Medicine, National University Health System, National University of Singapore, Singapore

Abstract

Since its identification in 1969, Enterovirus 71 (EV71) has been causing periodic outbreaks of infection in children worldwide and most prominently in the Asia-Pacific Region. Understanding the pathogenesis of Enterovirus 71 (EV71) is hampered by the virus's inability to infect small animals and replicate in their derived *in vitro* cultured cells. This manuscript describes the phenotypic and genotypic characteristics of two selected EV71 strains (EV71:TLLm and EV71:TLLmv), which have been adapted to replicate in mouse-derived NIH/3T3 cells, in contrast to the original parental virus which is only able to replicate in primate cell lines. The EV71:TLLm strain exhibited productive infection in all primate and rodent cell lines tested, while EV71:TLLmv exhibited greater preference for mouse cell lines. EV71:TLLmv displayed higher degree of adaptation and temperature adaptability in NIH/3T3 cells than in Vero cells, suggesting much higher fitness in NIH/3T3 cells. In comparison with the parental EV71:BS strain, the adapted strains accumulated multiple adaptive mutations in the genome resulting in amino acid substitutions, most notably in the capsid-encoding region (P1) and viral RNA-dependent RNA polymerase (3D). Two mutations, E167D and L169F, were mapped to the VP1 canyon that binds the SCARB2 receptor on host cells. Another two mutations, S135T and K140I, were located in the VP2 neutralization epitope spanning amino acids 136–150. This is the first report of human EV71 with the ability to productively infect rodent cell lines *in vitro*.

Citation: Victorio CBL, Xu Y, Ng Q, Chow VTK, Chua KB (2014) Phenotypic and Genotypic Characteristics of Novel Mouse Cell Line (NIH/3T3)-Adapted Human Enterovirus 71 Strains (EV71:TLLm and EV71:TLLmv). PLoS ONE 9(3): e92719. doi:10.1371/journal.pone.0092719

Editor: Herman Tse, The University of Hong Kong, Hong Kong

Received: December 5, 2013; **Accepted:** February 25, 2014; **Published:** March 26, 2014

Copyright: © 2014 Victorio et al. This is an open-access article distributed under the terms of the Creative Commons Attribution License, which permits unrestricted use, distribution, and reproduction in any medium, provided the original author and source are credited.

Funding: The research was fully funded by Temasek LifeSciences Laboratory (TLL). The funder had no role in study design, data collection and analysis, or preparation of the manuscript. The authors have obtained permission from the institute to publish these results.

Competing Interests: The authors have declared that no competing interests exist.

* E-mail: chuakb@tll.org.sg

Introduction

Enterovirus 71 (EV71) is a small non-enveloped virus approximately 30 nm in diameter. The viral capsid exhibits icosahedral symmetry and is comprised of 60 identical units (protomers), with each consisting of four viral structural proteins VP1–VP4. The capsid surrounds a core of a single-stranded positive-sense RNA genome of 7,450 nucleotides (nt) long. The genome contains a single open reading frame which encodes a polyprotein of 2193 amino acids (aa) and is flanked by a long 5′ untranslated region (UTR) of 745 nt and a shorter 3′ UTR of 85 nt with a poly-A tract of variable length at its 3′ terminus. The polyprotein is divided into three regions, *i.e.* P1, P2 and P3. P1 encodes four viral structural proteins 1A–1D (VP4, VP2, VP3 and VP1); P2 and P3 encode seven non-structural proteins 2A–2C and 3A–3D [1–3].

EV71 causes an array of clinical diseases including hand, foot and mouth disease (HFMD), aseptic meningitis, encephalitis and poliomyelitis-like paralysis mainly in infants and young children [4,5]. The virus was first isolated from a child with acute encephalitis in California, USA in 1969, and subsequently characterized as a new serotype of the genus *Enterovirus* in 1974 [6]. Outbreaks of HFMD with or without neurologic complications and deaths were reported in various parts of the world [7–20]. Since 1997, EV71 infections have been a major public health burden and of constant epidemiologic concern in the Asia-Pacific

Region. An HFMD outbreak due to highly neurovirulent EV71 emerged in Malaysia resulting in 48 deaths in 1997 [21,22], followed by a larger outbreak that occurred in Taiwan in 1998 with more than 129,000 cases of HFMD, 405 severe infections and 78 deaths due to acute brainstem encephalomyelitis with neurogenic cardiac failure and pulmonary edema [23–26]. In People's Republic of China, 488,955 HFMD cases with 126 deaths were recorded in 2008 [27] and increased to 1,155,525 cases with 353 fatalities in 2009 [28]. In 2010, China experienced the largest ever HFMD outbreak with more than 1.7 million cases, 27,000 patients with severe neurologic complications, and 905 deaths [29].

Similar to other human enteroviruses, EV71 is unable to infect animals other than humans, although rhesus and cynomolgous monkeys can be experimentally infected [30–32]. Understanding its pathogenesis and development of specific therapeutics against the virus are hampered by the lack of suitable small animal models, because EV71 is unable to naturally infect small rodents. Attempts to establish mouse models of EV71 infection and disease have been made, mostly through virus adaptation by serial passages in young suckling mice [33–39]. Although some models were able to recapitulate symptoms of clinical illness, none has been reported to cause disease in immune-competent mice aged 2 weeks old or older. Moreover, clinical features of disease and

pathology of EV71 infections in humans and experimental monkeys could not be replicated in mice, with the exception of the immunocompromised interferon receptor-deficient AG129 mice [35].

RNA viruses, by virtue of their error-prone replication and high mutation rates [40–42], replicate as a swarm of related variant sequences known as *quasispecies* [43,44]. It is comprised of a master species exhibiting the highest fitness in a certain environment, and of a mutant spectrum composed of a collection of closely related mutant sequences with a certain probability distribution [44,45]. These endow RNA viruses with genome plasticity, which is reflected in their ability to quickly adapt to changing environments. Despite these endowments, there has been no report of human EV71 that possesses the ability to productively infect rodent-derived cell lines, until now. This manuscript details the phenotypic and genotypic characteristics of two selected mouse cell line (NIH/3T3)-adapted EV71 strains (EV71:TLLm and EV71:TLLmv), which have gained the ability to cause productive infection in cultured rodent cells due to adaptive mutations in the viral genomes. This is the first report of human-derived EV71 that have been successfully adapted to productively infect cell lines of mouse, hamster, and rat origin. EV71:TLLm and EV71:TLLmv represent novel EV71 strains with unique genomic sequences, which can be further applied in developing mouse models of EV71 infection.

Results

Primate Cell Lines but not Rodent Cell Lines were Permissible to Infection by EV71:BS

All primate cell lines used in this study were permissible to infection by EV71:BS virus. Human RD cells, as well as monkey Vero and COS-7 cells, exhibited full lytic cytopathic effects (CPE) within 48 hours post-infection (hpi) (Figure 1A, 1J, 1M), and viral antigens were detected in fixed infected cells (Figure 2A; data not shown for RD and Vero cells). Growth kinetic curves of the virus harvested from supernatant of various infected cell lines confirmed productive infection in RD, Vero, and COS-7 cells (Figure 3A). Virus harvested from RD and Vero cells reached an endpoint titer of 3×10^9 CCID₅₀/ml, while virus titer from COS-7 was 10^6 CCID₅₀/ml (Figure 3A). EV71:BS did not induce full CPE in HeLa and Hep-2 cells (Figure 1D, 1G), and the resulting viral titer was not measurable within the assay cut-off limit. However, viral antigen was detected by indirect immunofluorescent staining in both HeLa cells (Figure 2D) and Hep-2 cells (Figure 2G) indicating successful virus entry into the cells but inefficient or defective replication may have resulted in immeasurable virus titer.

All the rodent cell lines tested were determined to be non-permissible to EV71:BS infection. Lytic CPE of cells was absent following infection (Figure 4A, D, G, J, M), virus titer from supernatants was not measurable, and viral antigens could not be detected in inoculated cells (Figure 2J, M, P; Figure S4A, C, E).

The Mouse Cell (NIH/3T3)-adapted EV71:TLLm Virus Productively Infected both Primate and Rodent Cell Lines

EV71:TLLm was derived following serial passage of EV71:BS in NIH/3T3 mouse cell line for a minimum of 60 cycles. All primate and rodent cell lines tested, with the exception of NRK cells, were permissible to productive infection by EV71:TLLm. Full CPE was observed in RD, Vero, and COS-7 (Figure 1B, K, N), as well as NIH/3T3 and Neuro-2A cells (Figure 4B, E) at 48 hpi. High virus titer was measurable in supernatants harvested from all infected cell lines except NRK (Figure 3C, 3D), and the infected cells were tested positive for viral antigen by indirect

immunofluorescent assay (Figure 2B, E, H, K, Q). Full CPE and measurable viral titer were not observed in NRK cells (Figure 4N, 3D), but viral antigens could be detected (Figure 2N), indicating successful virus entry into NRK cells by EV71:TLLm but inefficient virus replication could have resulted in non-measurable virus titer.

The Mouse Cell (NIH/3T3)-adapted EV71:TLLmv Virus was able to Productively Infect Rodent Cell Lines but not All Primate Cell Lines

The EV71:TLLmv virus strain was derived from further passage of EV71:TLLm in NIH/3T3 cells for another 40 cycles. EV71:TLLmv caused lytic CPE in fewer number of cell lines - RD, Vero, NIH/3T3, Neuro-2A, and TCMK cells (Figure 3B), and full CPE was only observed in RD, NIH/3T3, and Neuro-2A cells (Figure 1C; 4C, F). TCMK, CHO-K1 and NRK cells were also noted to be permissible to infection without progressing to full CPE (Figure 4I, L, O), as shown by positive viral antigen detection in the infected cells (Figure 2L, O, R).

On the other hand, the primate cell lines HeLa, Hep-2, and COS-7 were observed to be non-permissible to EV71:TLLmv infection, as shown by the absence of CPE (Figure 1F, 1I, 1O), immeasurable virus titers (Figure 3B), and negative viral antigen detection (Figure 2C, F, I).

EV71:TLLmv Virus Exhibited a Higher Degree of Adaptation to NIH/3T3 Cells, While EV71:TLLm was More Adapted to Replicate in Vero Cells

The amount of viable virus in supernatants harvested from infected cells at various time points was determined by enumerating the virus titer in both Vero and NIH/3T3 cells. The relative reproductive ratio (*RRR*), calculated by taking the ratio of virus titer values assayed in NIH/3T3 to the titer values assayed in Vero, was used as a surrogate measure of the degree of virus adaptation to NIH/3T3 cells. The parental EV71:BS virus displayed highly negative *RRR* values for RD, Vero, and COS-7 (Figure 5A), indicating that the virus titer assayed in Vero cells far exceeds the titer assayed in NIH/3T3 cells. The relative reproductive ratio values for other cell lines could not be determined since the virus titers could not be measured. On the other hand, EV71:TLLmv virus exhibited positive *RRR* values, with the exception of virus propagated in Vero cells (Figure 5B). The positive *RRR* values were indicative of more efficient replication, and therefore higher titer values, in NIH/3T3 cells compared to Vero cells. The negative *RRR* value determined for EV71:TLLmv harvested from Vero cells was consistent with the observed slow growth kinetics (Figure 3B) and lower virus titer. EV71:TLLm exhibited negative *RRR* values (Figure 5C, D), although of lesser degree than the *RRR* values for EV71:BS. This suggested that although EV71:TLLm could productively infect a few rodent cell lines, it was still more adapted to replicate in Vero than NIH/3T3 cells.

EV71:TLLm Exhibited Better Adaptability to Changing Temperatures than EV71:TLLmv

Vero and NIH/3T3 cells infected with the parental EV71:BS and the derived NIH/3T3-adapted EV71:TLLm and EV71:TLLmv strains were incubated at various temperatures - 30°C, 37°C, and 39°C, to determine virus adaptability to temperature variation or changes. EV71:BS displayed the most limited adaptability, with full CPE observed only in Vero cells incubated at 37°C (Figure S2B; Table 1). EV71:TLLmv displayed moderate adaptability, based on the observed full CPE induction

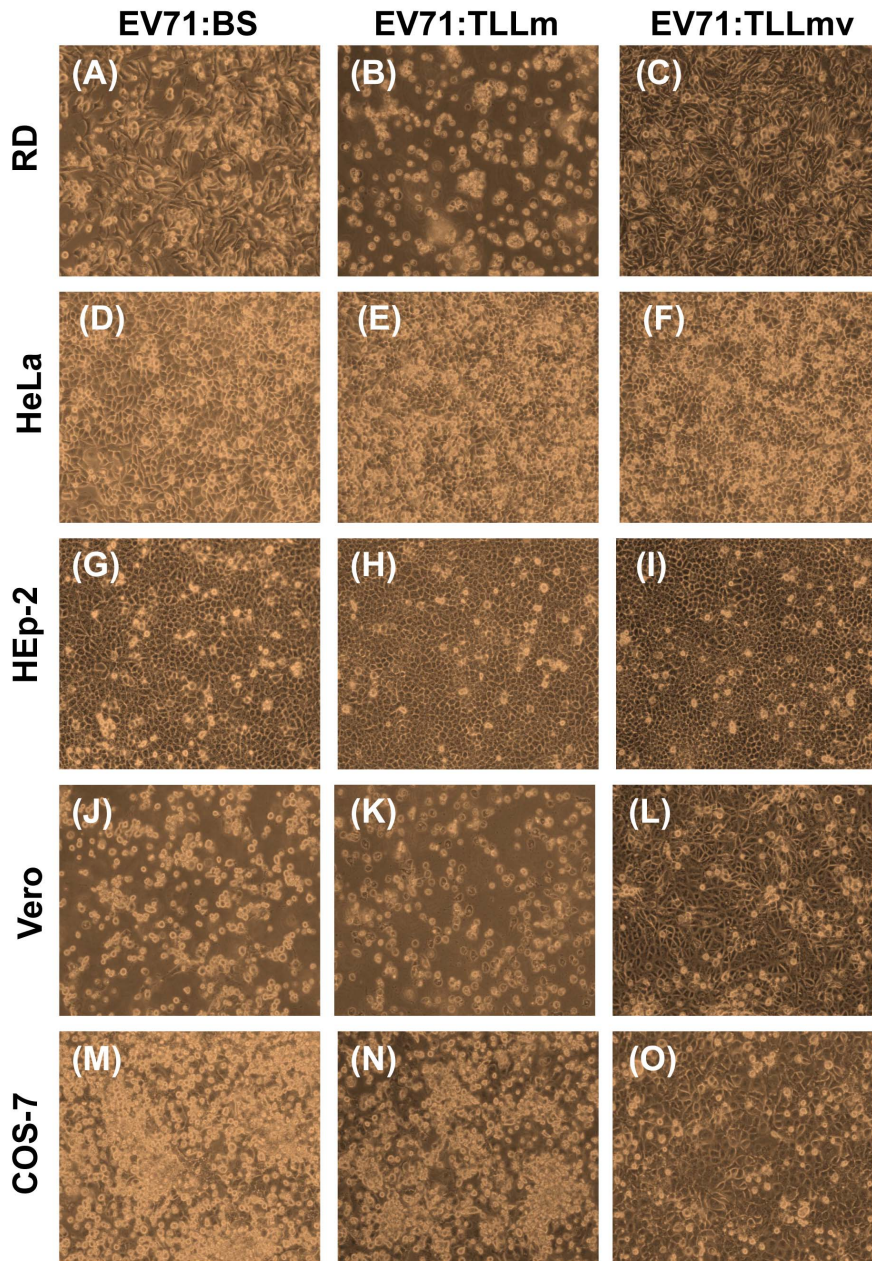


Figure 1. Cytopathic Effects (CPE) observed following virus infection of various primate cell lines. Primate cells: RD cells (A–C), HeLa cells (D–F), HEp-2 cells (G–I), Vero cells (J–L), and COS-7 cells (M–O) infected with 1 MOI of either EV71:BS (A, D, G, J, M), EV71:TLLm (B, E, H, K, N), or EV71:TLLmv (C, F, I, L, O) virus were observed at 48 hpi for cytopathic effects or death of the cell monolayer. Images are representative of results in three independent experiments.

doi:10.1371/journal.pone.0092719.g001

in Vero cells at 37°C (Figure S2B) and in NIH/3T3 cells in both 37°C and 39°C (Figure S2A, S3A; Table 1). EV71:TLLm, on the other hand, displayed the greatest adaptability, where it induced full CPE in Vero cells for all incubation temperatures (Figure S1B, S2B, S3B) though only at 37°C in NIH/3T3 cells (Figure S2A; Table 1).

The Viral Genomes of EV71:TLLm and EV71:TLLmv Accumulated Multiple Missense Mutations as a Result of Adaptation to NIH/3T3 Cells

Viral RNA of EV71:BS, EV71:TLLm, EV71:TLLmv were subjected to Sanger sequencing to determine the consensus

genome sequence and identify possible adaptive mutations arising from the adaptation process in NIH/3T3 cells. The consensus sequences of the genomes representing dominant population of the quasi-species have been deposited in the GenBank, NCBI (National Center for Biotechnology Information). Alignment of the full genome sequences of EV71:TLLm (GenBank Accession No. KF514879) against EV71:BS (GenBank Accession No. KF514878) revealed 60 nucleotide mutations, 21 of which resulted in amino acid substitutions (Table 2). On the other hand, 83 mutations with 36 amino acid substitutions, were noted between the genomes of EV71:TLLmv (Genbank Accession No. KF514880) and EV71:BS. Majority of the missense mutations

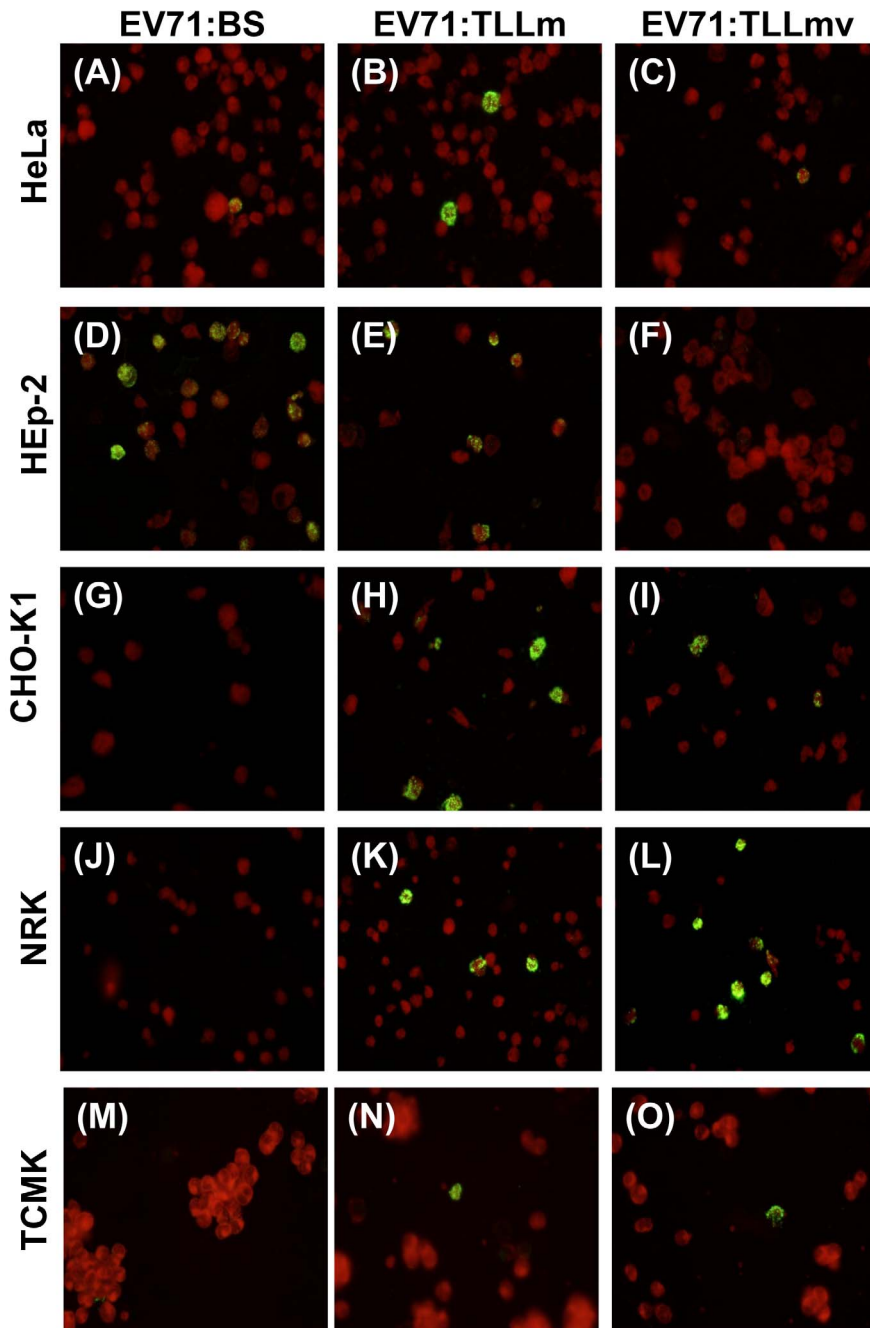


Figure 2. Virus antigen detection in cell lines infected with EV71:BS, EV71:TLLm and EV71:TLLmv. Overnight seeded mammalian cell lines: COS-7 (A–C); HeLa (D–F), HEp-2 (G–I), CHO-K1 (J–L), NRK (M–O), and TCMK (P–R), were infected with 1 MOI of respective virus. Cells were harvested at 48 hpi, coated onto Teflon slides and fixed in cold acetone. Cells were probed with pan-enterovirus antibody and stained with FITC-conjugated anti-mouse IgG. Images are representative of two independent experiments. doi:10.1371/journal.pone.0092719.g002

were located in the P1 (capsid protein genes) region (Table 2), particularly within the VP1 protein gene (Table 3).

Amino acid changes were also observed within the P2 and P3 regions, most notably in the RNA-dependent RNA polymerase (3D). EV71:TLLm acquired four amino acid changes, mostly in the palm and thumb domains of the enzyme (Table 4). EV71:TLLmv, on the other hand, accumulated eight amino acid changes, mostly also in the palm and thumb domains of the polymerase. Nucleotide mutations were also observed in the 5' untranslated region (UTR) of the genome. Apart from base

changes, a 1-base insertion was found in EV71:TLLm, while a 4-bp insertion and a 20-bp deletion were observed in EV71:TLLmv 5'UTR (Tables 2 and 3). On the other hand, no amino acid substitutions were observed in the VP3 and 3A regions of EV71:TLLm, as well as in the 3'UTR of both EV71:TLLm and EV71:TLLmv.

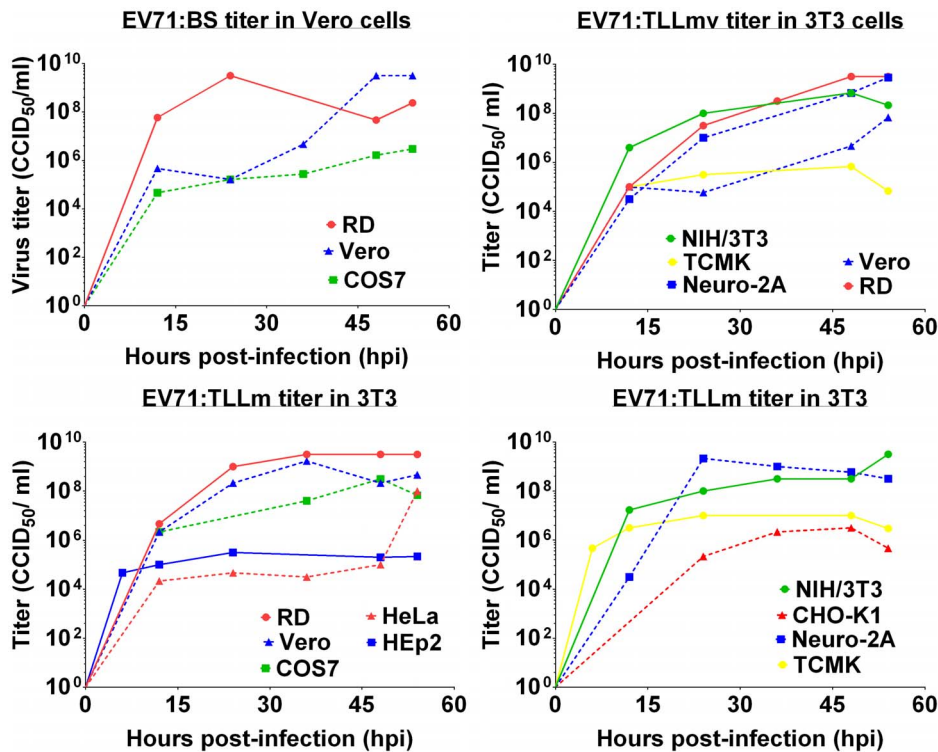


Figure 3. Growth kinetics of EV71:BS, EV71:TLLm, and EV71:TLLmv determined in NIH/3T3 and Vero cells. Supernatants from various mammalian cells infected with 1 MOI of respective virus were harvested at various time points and subjected to titration and enumerated using the Reed and Muench method. (A) EV71:BS virus titer determined in Vero cells. (B) EV71:TLLmv virus titer determined in NIH/3T3 cells. (C, D) EV71:TLLm virus titer determined in NIH/3T3 cells. Growth curves from cell lines that did not exhibit productive infection are not shown. doi:10.1371/journal.pone.0092719.g003

Transfection of EV71:BS Viral RNA into Murine Cells Resulted in Productive Infection but the Virus Progeny could not Re-infect the Same Mouse Cells

Vero and NIH/3T3 cells transfected with viral RNA exhibited full CPE at 7 days post-transfection (dpt) (data not shown). Viral antigens were detected in NIH/3T3 cells transfected with viral RNA of EV71:BS (Figure S4B), but not in NIH/3T3 cells subjected to infection with the virus (Figure S4A). Virus supernatants re-inoculated onto fresh Vero and NIH/3T3 cells resulted in productive infection (100% CPE) only in Vero but not in NIH/3T3 cells (Figure 6A), and viral antigen detection confirmed infection in Vero cells, but not NIH/3T3 (Figure 6B).

Discussion

Sequential passage of the human EV71 isolate (EV71:BS) generated virus strains that gained the ability to infect *in vitro* cultured rodent cell lines. The mouse adherent fibroblast cell line NIH/3T3, which was derived from the NIH/Swiss mouse embryo [46], was used to adapt the human EV71 strain to infect rodent cells. We report two such NIH/3T3-adapted strains - EV71:TLLm and EV71:TLLmv, where EV71:TLLm represents the early stage (passage number 60) and EV71:TLLmv represents the late stage (passage number 100) of the adaptation process. Based on the appearance of virus-induced CPE, measurement of high titer values, and positive detection of viral antigen through immunostaining, we categorized the virus-induced infection in cells as either productive or non-productive. Productive infection exhibits positive viral antigen detection as well as high virus titers, regardless of observation of CPE. On the other hand, non-

productive infection is characterized by immeasurable virus titer at cut-off assay limit despite viral antigen detection and/or observation of CPE.

Whereas the clinical isolate EV71:BS infects only primate cell lines, EV71:TLLm productively infects both primate and rodent cell lines. It is worth noting that although EV71:TLLm virus has successfully achieved the ability to infect rodent cells, the degree of adaptation to NIH/3T3 cells is less pronounced. The virus titer determined using Vero cells is much higher than that determined in NIH/3T3 cells, as indicated by negative values in relative replication rates (RRR) assay (Figure 5C, D). In addition, EV71:TLLm successfully infects Vero cells leading to full CPE at various incubation temperatures whereas it can only achieve full CPE in infected NIH/3T3 at 37°C (Table 1). Further adaptation in mouse cells, which yielded the EV71:TLLmv virus, resulted in a virus strain that displays a higher degree of adaptation to mouse cells (Figure 5B) but at the cost of narrowing down the spectrum of permissible host cells. EV71:TLLmv does not infect primate cell lines as effectively as mouse cells although it exhibits successful infection leading to full CPE of NIH/3T3 cells incubated at a broader range of temperatures (Table 1). However, compared to the predecessor EV71:TLLm, EV71:TLLmv seemed to have lost the ability to enter and replicate in monkey kidney COS-7 cells, as well as human HeLa and Hep-2 cells (Figure 3B–C; 2B–C, E–F, H–I). It also lost the ability to replicate efficiently within hamster CHO-K1 and rat NRK cells (Figure 3B–D; 2K–L, N–O). These observations indicate that further passage of the virus in NIH/3T3 cells increases the degree of adaptation in mouse cells at the cost of losing infective ability in cell lines of other origin.

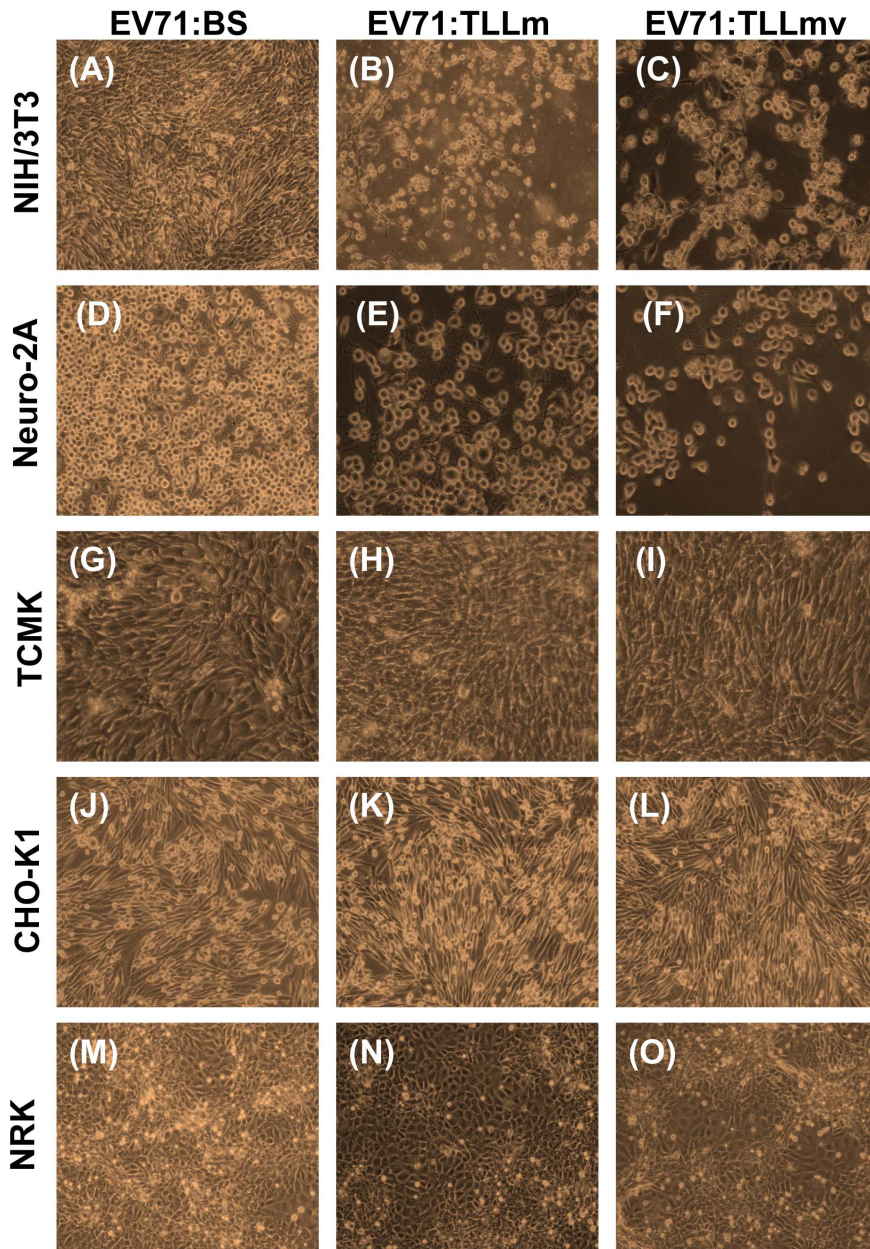


Figure 4. Cytopathic Effects (CPE) observed following virus infection of various rodent cell lines. Rodent cells: NIH/3T3 cells (A–C), Neuro-2A cells (D–F), TCMK cells (G–I), CHO-K1 cells (J–L), and NRK cells (M–O) infected with 1 MOI of either EV71:BS (A, D, G, J, M), EV71:TLLm (B, E, H, K, N), or EV71:TLLmv (C, F, I, L, O) viruses were observed at 48 hpi for cytopathic effects or death of the cell monolayer. Images are representative of results from three independent experiments.
doi:10.1371/journal.pone.0092719.g004

Although it is not possible to pinpoint which amino acid substitutions are adaptive to the mouse NIH/3T3 host cell, and this subject is not covered in this manuscript, viral whole genome sequencing may shed light to potential adaptive mechanisms. Most of the amino acid substitutions identified reside in the P1 (capsid) and RNA polymerase (3D) proteins (Table 2, 3), suggesting possible altered virus protein activity in host cell entry and replication. The accumulation of mutations in the P1 region is expected from the acquired ability of EV71:TLLm and EV71:TLLmv strains to infect new host cells. Capsid proteins form the structural context with which the virus initiates interaction with the permissive host cell through the virus receptor,

which had been identified recently as Scavenger Receptor Class B Member 2 (SCARB2) [47] and later characterized as the main virus uncoating receptor of EV71 [48] and which is also utilized by some members of Human Enterovirus A (HEV-A) species. The human SCARB2 protein shares approximately 99% sequence identity with that of other primates. On the other hand, mouse SCARB2 protein exhibits 15% sequence dissimilarity compared to the primate protein [49], implying significant structural deviations from primate SCARB2 and perhaps contributing to the recalcitrance of rodent cells to native EV71 infection. It is plausible that adaptive mutations in the virus capsid may render the virus

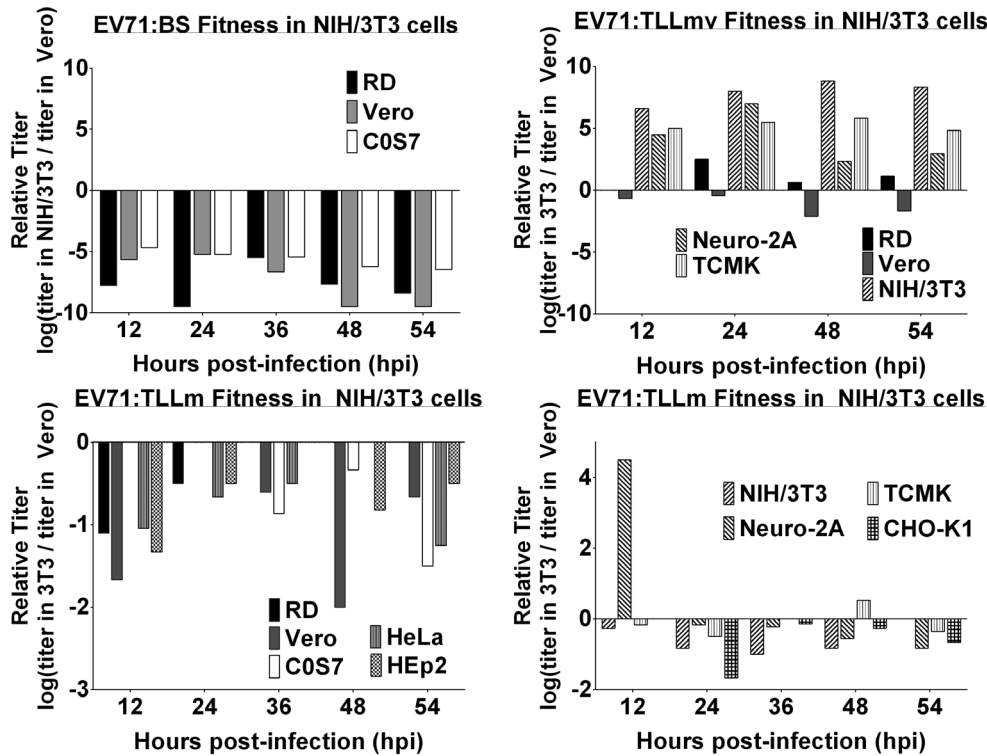


Figure 5. Virus fitness assessment of EV71:BS, EV71:TLLm, and EV71:TLLmv in NIH/3T3 determined by the titer ratio. Virus titer determined separately in NIH/3T3 and Vero cells were used to calculate the virus fitness as $\log[(\text{titer in NIH/3T3 cells})/(\text{titer in Vero cells})]$. Virus fitness of (A) EV71:BS, (B) Ev71:TLLmv, and (C, D) EV71:TLLm were calculated from the virus titer values shown in Figure 3. Virus fitness assays obtained from cell lines that did not exhibit productive infection are not shown. doi:10.1371/journal.pone.0092719.g005

competent to bind the mouse cell receptor and result in successful entry and infection of novel hosts.

Mapping of the capsid protein mutations indicate that majority of the identified amino acid substitutions in the viral P1 region reside in exposed regions of the protein (Figure S5), specifically in the B–C, D–E, E–F, and G–H loops on the surface of VP1. The VP1 residues 150–180 harbour the viral capsid canyon that engages SCARB2 protein. This region centred at Gln-172 contains a major VP1 neutralization epitope at amino acids 163–177 [32]. Both EV71:TLLm and EV71:TLLmv exhibited substitutions E167D and L169F in the E–F loop of the VP1 canyon (Figure S5A–B), loci which have not been previously reported.

Other significant amino acid substitutions near the SCARB2 docking site include N104D within the B–C loop and S241L in the G–H loop, which are located within a 20 Å radius from Gln-172. The VP1 S241L mutation, in association with the K244E, had been previously reported arising from mouse passage of a CHO cell line-adapted EV71 [50]. This mutation, in combination with a VP2 K149I, was found to be associated with a non-virulent phenotype in 5-day mouse pups. However, a reverse mutation at VP1 241 from Leu to Ser [51] was reported arising from adaptation in NOD/SCID mouse brain tissues and found to be associated with a mouse virulent phenotype. The VP1 E145A mutation, which is far from the SCARB2 docking site and located

Table 1. Assessment of virus adaptability of EV71:BS, EV71:TLLm and EV71:TLLmv grown in NIH/3T3 and Vero cells to various incubation temperatures.

Incubation Temperature (°C)	Induction of full cytopathic effect (CPE) within 48 hours following infection ¹					
	EV71:BS		EV71:TLLm		EV71:TLLmv	
	Vero	NIH/3T3	Vero	NIH/3T3	Vero	NIH/3T3
30	– ²	–	+	(30%) ³	–	–
37	+ ³	–	+	+	+	+
39	(20%) ⁴	–	+	(<10%) ³	–	+

¹Infected cells were observed daily for signs of lytic cell death and time of appearance of full CPE.
²indicates absence of full CPE in infected cells.
³indicates observation of full CPE.
⁴indicates absence of full CPE, while number in parentheses indicates the maximum degree of CPE observed in cells.
 doi:10.1371/journal.pone.0092719.t001

Table 2. Nucleotide and amino acid changes in the genomes of EV71:TLLm and EV71:TLLmv compared to EV71:BS.

Genomic region	EV71:BS vs EV71:TLLm		EV71:BS vs EV71:TLLmv	
	No. nucleotide changes	No. amino acid changes	No. nucleotide changes	No. amino acid changes
5' UTR ⁵	11	n/a	11	n/a
	1-bp INS ⁶		4-bp INS ¹⁸	
			20-bp DEL ⁷	
P1	22	12	39	22
P2	11	2	11	2
P3	16	7	22	12
3' UTR ⁸	0	n/a	0	n/a
total	60	21	83	36

⁵5'UTR – 5' Untranslated Region.⁶INS – Insertion.⁷DEL – Deletion.⁸3'UTR – 3' Untranslated Region.

doi:10.1371/journal.pone.0092719.t002

in the D–E loop, is another candidate for conferring the ability to infect murine cells. The VP1 145 mutation had been previously reported [34,37] and a single E145A mutation leads to virulence in NOD/SCID mice [51]. Another mutation in VP1 of a C4 genotype EV71, Q145E, was associated with virulence in 5-day old mice [52]. The mouse cell-adaptive mutations in VP2, particularly those within the neutralizing epitope of residues 136–150 [53], may also contribute to the virus ability to infect rodent cells. Two substitutions in VP2 E-F loop were observed in EV71:TLLm (Figure S6C), while three substitutions were present in EV71:TLLmv (Figure S5D). None of these mutations have been previously described, although a nearby locus at VP2 149 in the E-F loop had been mentioned in the literature [34,50,54] and described as an adaptive mutation to passage in PSGL-1 overexpressing cells [55].

To explore the possible role of the P1 region mutations in binding the virus receptor for host cell entry, EV71:BS viral RNA was transfected into murine cells. Direct introduction of EV71:BS RNA into the mouse cell cytoplasm results to productive infection in NIH/3T3 cells, as suggested by the observation of virus-induced CPE and measurable virus titers in the culture supernatant as assayed in Vero cells (Figure S6). Re-inoculation of the virus supernatant onto fresh NIH/3T3 cells, however, fails to induce productive infection (Figure 6A) and no viral antigens were detected (Figure S4H). Similarly, transfection of EV71:BS RNA into Neuro-2A cells, but not direct virus infection, resulted in positive antigen staining in Neuro-2A cells (Figure S4C, S4D) and measurable virus titers (Figure S6). Virus supernatants passaged onto fresh Vero and NIH/3T3 cells resulted to positive antigen staining in Vero (Figure S4I) but not in NIH/3T3 cells (Figure S4J). These data indicate that circumventing the requirement of receptor engagement for host cell entry led to successful infection and production of virus progenies in NIH3T3 and Neuro-2A cells. These data also support that human EV71:BS cannot successfully enter mouse NIH/3T3 and Neuro-2A cells through murine cellular receptor. Moreover, these data suggest that mutations within the P1 region of EV71:TLLm and EV71:TLLmv genomes confer the virus with the ability for efficient receptor engagement, and consequently host cell entry.

Several amino acid mutations were also observed in the P2 and P3 regions, which encode virus proteins that are crucial for virus replication and hijacking the host cell protein translation

machinery [56]. These adaptive mutations may function in optimizing EV71 genome replication and translation within mouse cells. The viral 3D protein alone accumulated 8 amino acid substitutions in EV71:TLLmv and 4 in EV71:TLLm, and both strains exhibited 1 mutation each in 3B and 2 mutations each in 3C. Direct inoculation of viral RNA into TCMK cells give insight into the possible role of the adaptive mutations in the nonstructural proteins of the virus. Although TCMK cells have been shown to be permissible to EV71:TLLm and EV71:TLLmv infection (Figure 3B, D; 4Q, R), transfection of EV71:BS viral RNA into TCMK cells did not result to successful infection. Viral antigen signals were not detected in infected and transfected cells (Figure S4E–F), and passage of virus supernatant onto fresh NIH/3T3 and Vero cells did not yield positive viral antigen detection (Figure S4K, L). Moreover, there was no assayable virus titer in both infected and transfected cells (Figure S6). These data suggest that apart from mutations in the capsid region, mutations within the P2 and P3 regions, which are found in EV71:TLLm and EV71:TLLmv, are required to successfully infect TCMK cells. The specific role of these adaptive mutations, which is the focus of ongoing studies, is beyond the scope of this manuscript.

To our knowledge, this is the first report of EV71 strains originally derived from human clinical sample that have successfully gained the ability to productively infect several rodent cell lines following successive passages in a mouse cell line. The relatively high mutation rates during RNA replication results in variant genomes that serve as genetic reservoirs of phenotypic traits for future adaptive potential, and the consequential replication as a quasispecies distribution [57,58] leads to the dynamic plasticity of RNA viral genomes conferring adaptability to changing environments [59,60]. Although EV71 infecting suckling mice [34,37,38,51] and other rodents (e.g. gerbils) [39] have been reported previously, none was reported to productively infect *in vitro* cultured rodent cells. This may be due to the high genetic barrier associated with major changes in phenotype and host range [58]. Interestingly, our group is the first to report a large number of adaptive mutations within the consensus full genome sequence of EV71. Whereas previously documented mouse-adapted EV71 reported less than 10 amino acid substitutions in the genome [34,38,51], we report 21 in EV71:TLLm and 36 in EV71:TLLmv, still more than the most number of adaptive mutations previously identified [37]. These suggest that few

Table 3. Adaptive mutations observed in the 5'UTR and P1 regions of EV71:TLLm and EV71:TLLmv viral genomes.

EV71:BS vs EV71:TLLm		EV71:BS vs EV71:TLLmv	
Amino acid changes		Amino acid changes	
Genome region	Nucleotide changes	Polyprotein ²	Mature protein ¹⁰
Cloverleaf		Genome region	
IRES ¹¹		Cloverleaf	
		IRES	
	A 141 G		C 140 G
	G 195 C		A 141 C
	T 209 C		T 209 C
	G 258 A		G 258 A
	C 370 T		C 370 T
	G 448 A	Not applicable	G 448 A
	T 502 C		A 502 C
	C 709 T		G 675 T
	A 671 T		T 677 C
	G 675 T		C 687 T
	T 678 INS ¹⁰		C 709 T
			678–681 INS
			726–745 DEL ¹³
VP4	A 809 G	E 21 G	A 809 G
	G 1359 A	V 204 I	G 1359 A
	G 1385 C	S 213 T	G 1385 C
	A 1400 T	K 218 I	A 1400 T
		T 1428 C	T 1428 C
		G 1429 C	G 1429 C
		G 1900 C	G 1900 C
		A 2287 G	A 2287 G
		A 2421 G	A 2421 G
		T 2462 C	T 2462 C
		C 2530 A	C 2530 A
		A 2734 G	A 2719 G
		A 2752 G	T 2724 A
		A 2876 G	C 2725 T
		A 2943 T	A 2734 G
		C 2947 T	A 2752 G
		C 3165 T	A 2753 G
			A 2876 G
			A 2943 T
			C 2947 T
			E 21 G
			V 204 I
			S 213 T
			K 218 I
			E 228 P
			E 228 P
			A 385 P
			T 514 A
			I 558 M
			V 572 A
			Q 595 K
			I 658 V
			D 659 E
			I 660 F
			K 663 E
			N 669 G
			E 710 A
			E 732 D
			E 150 P
			A 62 P
			T 191 A
			I 235 M
			V 7 A
			Q 30 K
			I 93 V
			D 94 E
			I 95 F
			K 98 E
			N 104 G
			E 145 A
			E 167 D
			E 167 D
			L 734 F
			S 241 L
			E 145 A
			E 167 D
			L 734 F
			L 169 F

Table 4. Adaptive mutations observed in the P2 and P3 regions of EV71:TLLm and EV71:TLLmv viral genomes.

EV71:BS vs EV71:TLLm ¹⁴				EV71:BS vs EV71:TLLmv ¹¹			
Amino acid changes				Amino acid changes			
Genome region	Nucleotide changes	Polyprotein ¹⁵	Mature protein ¹⁶	Genome region	Nucleotide changes	Polyprotein	Mature protein
2A	G 3722 A	G 992 E	G 130 E	2A	G 3722 A	G 992 E	G 130 E
2C	A 4366 G	T 1207 A	T 96 A	2C	A 4366 G	T 1207 A	T 96 A
3A					C 5117 T	A 1457 V	A 17 V
3B	T 5357 C	L 1537 P	L 11 P	3B	T 5357 C	L 1537 P	L 11 P
3C	A 5557 G	I 1604 V	I 56 V	3C	A 5557 G	I 1604 V	I 56 V
	A 5569 G	I 1608 V	I 60 V		A 5569 G	I 1608 V	I 60 V
3D	A 6211 G	N 1822 D	N 91 D	3D	A 6070 T	T 1775 S	T 44 S ¹⁷
	T 6835 A	S 2030 T	S 299 T ⁴		T 6137 C	V 1797 A	V 66 A ³
	A 7128 G	R 2127 S	R 396 S ⁵		A 6211 G	N 1822 D	N 91 D
	T 7247 C	V 2167 A	V 436 A ⁵		C 6404 G	S 1886 C	S 155 C
					T 6592 G	W 1949 G	W 218 G ¹⁸
					T 6835 A	S 2030 T	S 299 T ⁴
					A 7128 G	R 2127 S	R 396 S ¹⁹
					T 7247 C	V 2167 A	V 436 A ⁵

¹⁴Mutations are based on alignment with the reference EV71:BS genome.

¹⁵Numbering of amino acids in the uncleaved polyprotein prior to maturation.

¹⁶Numbering of amino acids in the mature protein.

¹⁷Mutation located in the Ring finger domain of the RNA-dependent RNA Polymerase.

¹⁸Mutation located in the Palm domain of the RNA-dependent RNA Polymerase.

¹⁹Mutation located in the Thumb domain of the RNA-dependent RNA Polymerase.

doi:10.1371/journal.pone.0092719.t004

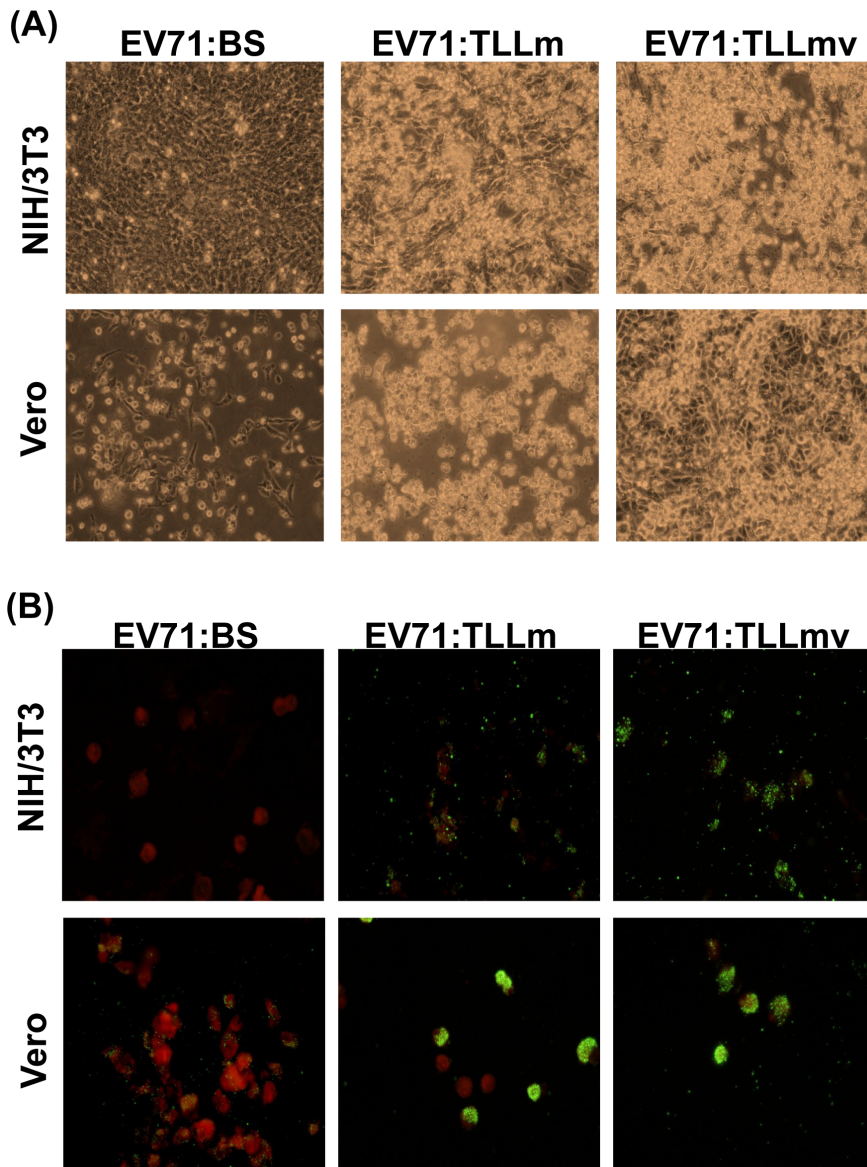


Figure 6. Transfection of NIH/3T3 with EV71:BS viral RNA induces productive infection. Overnight seeded NIH/3T3 and Vero cells were inoculated with virus supernatant harvested from NIH/3T3 cells previously transfected viral RNA extracted from EV71:BS, EV71:TLLm, and EV71:TLLmv. (A) Cells were imaged using inverted light microscope at 24 hpi to observe induced CPE. (B) Cells were harvested at 7 dpi, coated onto Teflon slides, probed with pan-enterovirus antibody, and stained with anti-mouse FITC-conjugated antibody. doi:10.1371/journal.pone.0092719.g006

For temperature adaptation assays, inoculated Vero and NIH/3T3 cells were incubated at 30°C, 37°C, and 39°C and observed daily for appearance of CPE. Respective culture supernatants were harvested at 48 hpi and stored in cryovials at -80°C until further use.

Various mammalian cell lines, i.e. RD, HeLa, and HEp-2 (human), Vero and COS-7 (monkey), NIH/3T3, Neuro-2A, and TCMK (mouse), CHO-K1 (hamster), and NRK cells (rat), were infected with either parental EV71:BS or derived NIH/3T3-adapted EV71 strains at MOI (multiplicity of infection) of 1 and incubated at 37°C for 10 days. Cultures were observed daily for appearance of CPE.

C. Determination of Virus Titer and Relative Replication Rates (RRR)

Virus supernatants were subjected to endpoint titration and assayed in both NIH/3T3 and Vero cells. The virus titer was enumerated using the Reed and Muench method [61] and the Reed and Muench calculator [62]. Briefly, NIH/3T3 (1×10^4 cells per well) and Vero cells (4×10^3 cells per well) were seeded overnight in a 96-well plate. Frozen virus thawed to room temperature were diluted (10^{-1}) in sterile 1% aqueous sodium deoxycholate (Sigma Aldrich, USA), and vigorously mixed for 15 minutes to disaggregate virus. Disaggregated virus was subjected to ten-fold serial dilution in maintenance medium, and 100 μl diluted virus from 10^{-3} dilution onwards was added onto each well of cells. Plates were incubated at 37°C and observed daily under inverted light microscopy for the appearance of distinct CPE.

Virus titer was reported as 50% cell culture-infectious doses per volume (CCID₅₀/ml).

To assess the degree of adaptation of EV71:TLLm and EV71:TLLmv in NIH/3T3 cells, virus supernatants harvested from previously infected primate and rodent cell lines were subjected to virus titer assay using both NIH/3T3 and Vero cells. The titer ratio used to measure *relative replication rates* (RRR) in NIH/3T3 and Vero cells was calculated using the following formula:

$$RRR = \log(A/B)$$

where *A* is the virus titer assayed in NIH/3T3 cells, and *B* is the virus titer assayed in Vero cells.

D. Virus Antigen Detection by Immunofluorescence Assay

For infected cells that did not exhibit significant CPE, immunofluorescence (IF) staining was performed to verify infection. Cells were trypsinized at 72 hpi, washed twice in sterile PBS, and coated onto Teflon slides (Erie, USA). Slides were air-dried inside the biosafety cabinet and UV-treated for 15 minutes to inactivate live virus prior to fixation in cold acetone at 4°C for 10 minutes. Slides were probed with pan-Enterovirus antibody (Merck Millipore, USA) and subsequently with FITC-conjugated mouse IgG (DAKO Cytomation, Denmark) mixed with 0.01% (v/v) Evan's blue counter stain.

E. Transfection of Cells with EV71 Viral RNA

Vero and NIH/3T3 cells (3 × 10⁴ cells per well) seeded overnight in 24-well plates were transfected with viral RNA extracted from 4 × 10⁶ CCID₅₀ virus using Lipofectamine 2000 (Life technologies, USA) following the manufacturer's protocol. RNA from EV71:BS, EV71:TLLm, and EV71:TLLmv was extracted using Viral RNA kit (Qiagen, Germany) and incubated with Lipofectamine 2000 on cells for 6 hours at 37°C. Transfected cells were observed daily for appearance of CPE. At 7 dpi, supernatant was harvested from infected cells and passaged onto freshly seeded Vero and NIH/3T3 cells. Cells were observed daily for appearance of CPE, and at 7 dpi, cells were trypsinized and processed for immunofluorescence viral antigen detection.

F. Full Genome Sequencing and Genetic Mapping of EV71 Strains

Viral RNA of EV71:BS, EV71:TLLm, and EV71:TLLmv strains was extracted using Viral RNA kit (Qiagen, Germany) and reverse-transcribed using Superscript II (SII-RT, Life Technologies, USA). The cDNA obtained was amplified with GoTaq Green (Promega, USA) and degenerate EV71 primers (primers' sequences are available upon request). The amplicon was purified using PCR clean up kit (Geneaid Biotech, Taiwan) and cloned into pZero2 vector (Lifetech, USA). Clones were selected from Kanamycin plates, inoculated into LB broth (50 µg/ml Kanamycin) and allowed to grow overnight at 37°C for plasmid extraction with QiaSpin Miniprep kit (Qiagen, Germany). Plasmids were subsequently sequenced by the BigDye terminator method (Applied Biosystems, USA) using the same primers. The 500-bp fragment sequences obtained were aligned using BioEdit v7.0.9.0 [63] against the whole genome sequence of an EV71 Singapore isolate 3799-SIN-98 (GenBank accession no. DQ341354.1) to reconstruct the full genome sequences of EV71:BS, EV71:TLLm, and EV71:TLLmv. Molecular modelling of the protomers of EV71:TLLm, and EV71:TLLmv was performed using Deepview/

Swiss pdbviewer ver. 3.7 (<http://expasy.org/spdbv/>) and the SWISS-MODEL server [64,65].

Supporting Information

Figure S1 Virus fitness assessment of EV71:BS, EV71:TLLm, and EV71:TLLmv in NIH/3T3 and Vero cells at 30°C. Overnight seeded (A) NIH/3T3 and (B) Vero cells infected with EV71:BS (a, d, g), EV71:TLLm (b, e, h), or EV71:TLLmv (c, f, i) were incubated at 30°C and observed under the light microscope with phase-contrast at 24 hpi (a–c), 48 hpi (d–f), and 72 hpi (g–i). Images taken are representative of two independent experiments. (TIF)

Figure S2 Virus fitness assessment of EV71:BS, EV71:TLLm, and EV71:TLLmv in NIH/3T3 and Vero cells at 37°C. Overnight seeded (A) NIH/3T3 and (B) Vero cells infected with EV71:BS (a, d, g), EV71:TLLm (b, e, h), or EV71:TLLmv (c, f, i) were incubated at 37°C and observed under the light microscope with phase-contrast at 24 hpi (a–c), 48 hpi (d–f), and 72 hpi (g–i). Images taken are representative of two independent experiments. (TIF)

Figure S3 Virus fitness assessment of EV71:BS, EV71:TLLm, and EV71:TLLmv in NIH/3T3 and Vero cells at 39°C. Overnight seeded (A) NIH/3T3 and (B) Vero cells infected with EV71:BS (a, d, g), EV71:TLLm (b, e, h), or EV71:TLLmv (c, f, i) were incubated at 39°C and observed under the light microscope with phase-contrast at 24 hpi (a–c), 48 hpi (d–f), and 72 hpi (g–i). Images taken are representative of two independent experiments. (TIF)

Figure S4 Transfection of murine cell lines NIH/3T3, Neuro-2A, and TCMK with EV71:BS viral RNA for evidence of virus replication. Overnight seeded NIH/3T3, Neuro-2A, and TCMK cells were either infected with 1000 CCID₅₀ of EV71:BS virus (A, C, E) or transfected with equivalent amounts of viral RNA (B, D, F), and harvested at 48 hpi for viral antigen detection. Virus in the supernatants were harvested at 7 dpi and passaged onto fresh Vero (G, I, K) and NIH/3T3 cells (H, J, L). Cells were harvested and stained for viral antigens at 48 hpi. (TIF)

Figure S5 Localization in VP1 and VP2 of adaptive mutations in the genomes of EV71:TLLm and EV71:TLLmv. Adaptive mutations observed in the VP1 (A, B) and VP2 (C, D) regions of EV71:TLLm (A, C) and EV71:TLLmv (B, D) were modelled using DeepView/SwissPDBviewer v3.7 and the 3D structure of EV71 capsid P1 region (PDB ID 4AED). The mutations were observed to be mostly localized to the surface-exposed loops of the protein. The B–C loop is shown in red; D–E loop in yellow; E–F loop in orange; and G–H loop in pink. (TIF)

Figure S6 Titer ratio in NIH/3T3 cells relative to titer in Vero cells of virus supernatant harvested from cells either transfected with EV71:BS viral RNA or infected with live virus. Supernatants from NIH/3T3, Neuro-2A, Vero, and TCMK either transfected with viral RNA or infected with live virus were harvested and subjected to virus enumeration by Reed- and Muench method. The ratio of the log(titer) determined in NIH/3T3 cells relative to the titer determined in Vero cells is shown. *3T3-TRANS*: RNA transfected NIH/3T3 cells; *3T3-INF*:

virus infected NIH/3T3 cells. Asterisks indicate Student's t-test with p-value <0.05. (TIF)

Acknowledgments

The mouse cell line-adapted strains of Enterovirus 71 were generated by Dr K. B. Chua, Temasek Lifesciences Laboratory.

References

- Alexander JP, Baden L, Pallansch MA, Anderson IJ (1994) Enterovirus 71 infections and neurologic disease—United States, 1977–1991. *J Infect Dis* 169: 905–908.
- Melnick JL (1996) Enteroviruses: Polioviruses, Coxsackieviruses, Echoviruses, and Newer Enteroviruses. In: Fields B N KDM, Howley P M, et al., editor. *Fields Virology*. Philadelphia.: Lippincott-Raven. 655–712.
- Bible JM, Iturriza-Gomara M, Megson B, Brown D, Pantelidis P, et al. (2008) Molecular epidemiology of human enterovirus 71 in the United Kingdom from 1998 to 2006. *J Clin Microbiol* 46: 3192–3200.
- Ooi MH, Wong SC, Lewthwaite P, Cardoso MJ, Solomon T (2010) Clinical features, diagnosis, and management of enterovirus 71. *Lancet Neurol* 9: 1097–1105.
- Solomon T, Lewthwaite P, Perera D, Cardoso MJ, McMinn P, et al. (2010) Virology, epidemiology, pathogenesis, and control of enterovirus 71. *Lancet Infect Dis* 10: 778–790.
- Schmidt NJ, Lennette EH, Ho HH (1974) An apparently new enterovirus isolated from patients with disease of the central nervous system. *J Infect Dis* 129: 304–309.
- Blomberg J, Lycke E, Ahlfors K, Johansson T, Wolontis S, et al. (1974) Letter: New enterovirus type associated with epidemic of aseptic meningitis and/or hand, foot, and mouth disease. *Lancet* 2: 112.
- Kennett ML, Birch CJ, Lewis FA, Yung AP, Locarnini SA, et al. (1974) Enterovirus type 71 infection in Melbourne. *Bull World Health Organ* 51: 609–615.
- Deibel R, Gross LL, Collins DN (1975) Isolation of a new enterovirus (38506). *Proc Soc Exp Biol Med* 148: 203–207.
- Hagiwara A, Tagaya I, Yoneyama T (1978) Epidemic of hand, foot and mouth disease associated with enterovirus 71 infection. *Intervirol* 9: 60–63.
- Chumakov M, Voroshilova M, Shindarov L, Lavrova I, Gracheva L, et al. (1979) Enterovirus 71 isolated from cases of epidemic poliomyelitis-like disease in Bulgaria. *Arch Virol* 60: 329–340.
- Shindarov LM, Chumakov MP, Voroshilova MK, Bojinov S, Vasilenko SM, et al. (1979) Epidemiological, clinical, and pathomorphological characteristics of epidemic poliomyelitis-like disease caused by enterovirus 71. *J Hyg Epidemiol Microbiol Immunol* 23: 284–295.
- Nagy G, Takátsy S, Kukán E, Mihály I, Dömök I (1982) Virological diagnosis of enterovirus type 71 infections: experiences gained during an epidemic of acute CNS diseases in Hungary in 1978. *Arch Virol* 71: 217–227.
- Chonmaitree T, Menegus MA, Schervish-Swierkosz EM, Schwalenstocker E (1981) Enterovirus 71 infection: report of an outbreak with two cases of paralysis and a review of the literature. *Pediatrics* 67: 489–493.
- Samuda GM, Chang WK, Yeung CY, Tang PS (1987) Monoplegia caused by Enterovirus 71: an outbreak in Hong Kong. *Pediatr Infect Dis J* 6: 206–208.
- Gilbert GL, Dickson KE, Waters MJ, Kennett ML, Land SA, et al. (1988) Outbreak of enterovirus 71 infection in Victoria, Australia, with a high incidence of neurologic involvement. *Pediatr Infect Dis J* 7: 484–488.
- Hayward JC, Gillespie SM, Kaplan KM, Packer R, Pallansch M, et al. (1989) Outbreak of poliomyelitis-like paralysis associated with enterovirus 71. *Pediatr Infect Dis J* 8: 611–616.
- Tagaya I, Takayama R, Hagiwara A (1981) A large-scale epidemic of hand, foot and mouth disease associated with enterovirus 71 infection in Japan in 1978. *Jpn J Med Sci Biol* 34: 191–196.
- Ishimaru Y, Nakano S, Yamaoka K, Takami S (1980) Outbreaks of hand, foot, and mouth disease by enterovirus 71. High incidence of complication disorders of central nervous system. *Arch Dis Child* 55: 583–588.
- Hagiwara A, Yoneyama T, Hashimoto I (1983) Isolation of a temperature-sensitive strain of enterovirus 71 with reduced neurovirulence for monkeys. *J Gen Virol* 64 (Pt 2): 499–502.
- Lum LC, Wong KT, Lam SK, Chua KB, Goh AY, et al. (1998) Fatal enterovirus 71 encephalomyelitis. *J Pediatr* 133: 795–798.
- Lum LC, Wong KT, Lam SK, Chua KB, Goh AY (1998) Neurogenic pulmonary oedema and enterovirus 71 encephalomyelitis. *Lancet* 352: 1391.
- Chang LY, Huang YC, Lin TY (1998) Fulminant neurogenic pulmonary oedema with hand, foot, and mouth disease. *Lancet* 352: 367–368.
- Yan JJ, Wang JR, Liu CC, Yang HB, Su IJ (2000) An outbreak of enterovirus 71 infection in Taiwan 1998: a comprehensive pathological, virological, and molecular study on a case of fulminant encephalitis. *J Clin Virol* 17: 13–22.
- Liu CC, Tseng HW, Wang SM, Wang JR, Su IJ (2000) An outbreak of enterovirus 71 infection in Taiwan, 1998: epidemiologic and clinical manifestations. *J Clin Virol* 17: 23–30.
- Wang JR, Tsai HP, Chen PF, Lai YJ, Yan JJ, et al. (2000) An outbreak of enterovirus 71 infection in Taiwan, 1998. II. Laboratory diagnosis and genetic analysis. *J Clin Virol* 17: 91–99.
- China C (2008) Report on the hand, foot and mouth disease outbreak in Fuyang City, Anhui Province and the prevention and control in China. Beijing, China: Office of the World Health Organization, China.
- Yang F, Zhang T, Hu Y, Wang X, Du J, et al. (2011) Survey of enterovirus infections from hand, foot and mouth disease outbreak in China, 2009. *Virol J* 8: 508.
- Zeng M, El Khatib NF, Tu S, Ren P, Xu S, et al. (2012) Seroepidemiology of Enterovirus 71 infection prior to the 2011 season in children in Shanghai. *J Clin Virol* 53: 285–289.
- Zhang Y, Cui W, Liu L, Wang J, Zhao H, et al. (2011) Pathogenesis study of enterovirus 71 infection in rhesus monkeys. *Lab Invest* 91: 1337–1350.
- Arita M, Shimizu H, Nagata N, Ami Y, Suzuki Y, et al. (2005) Temperature-sensitive mutants of enterovirus 71 show attenuation in cynomolgus monkeys. *J Gen Virol* 86: 1391–1401.
- Chen P, Song Z, Qi Y, Feng X, Xu N, et al. (2012) Molecular determinants of enterovirus 71 viral entry: cleft around GLN-172 on VP1 protein interacts with variable region on scavenger receptor B 2. *J Biol Chem* 287: 6406–6420.
- Chen YC, Yu CK, Wang YF, Liu CC, Su IJ, et al. (2004) A murine oral enterovirus 71 infection model with central nervous system involvement. *J Gen Virol* 85: 69–77.
- Chua BH, Phuektes P, Sanders SA, Nicholls PK, McMinn PC (2008) The molecular basis of mouse adaptation by human enterovirus 71. *J Gen Virol* 89: 1622–1632.
- Khong WX, Yan B, Yeo H, Tan EL, Lee JJ, et al. (2012) A non-mouse-adapted enterovirus 71 (EV71) strain exhibits neurotropism, causing neurological manifestations in a novel mouse model of EV71 infection. *J Virol* 86: 2121–2131.
- Ong KC, Badmanathan M, Devi S, Leong KL, Cardoso MJ, et al. (2008) Pathologic characterization of a murine model of human enterovirus 71 encephalomyelitis. *J Neuropathol Exp Neurol* 67: 532–542.
- Wang W, Duo J, Liu J, Ma C, Zhang L, et al. (2011) A mouse muscle-adapted enterovirus 71 strain with increased virulence in mice. *Microbes Infect* 13: 862–870.
- Wang YF, Chou CT, Lei HY, Liu CC, Wang SM, et al. (2004) A mouse-adapted enterovirus 71 strain causes neurological disease in mice after oral infection. *J Virol* 78: 7916–7924.
- Yao PP, Qian L, Xia Y, Xu F, Yang ZN, et al. (2012) Enterovirus 71-induced neurological disorders in young gerbils, *Meriones unguiculatus*: development and application of a neurological disease model. *PLoS One* 7: e51996.
- Borrego B, Novella IS, Giralt E, Andreu D, Domingo E (1993) Distinct repertoire of antigenic variants of foot-and-mouth disease virus in the presence or absence of immune selection. *J Virol* 67: 6071–6079.
- Burch CL, Chao L (1999) Evolution by small steps and rugged landscapes in the RNA virus phi6. *Genetics* 151: 921–927.
- Steinhauer DA, Domingo E, Holland JJ (1992) Lack of evidence for proofreading mechanisms associated with an RNA virus polymerase. *Gene* 122: 281–288.
- Biebricher C, Eigen M (2006) What is a Quasispecies. In: Domingo E, editor. *Quasispecies: Concept and Implications for Virology*. Heidelberg: Springer-Verlag. 1–31.
- Eigen M, Schuster P (1977) The hypercycle. A principle of natural self-organization. Part A: Emergence of the hypercycle. *Naturwissenschaften* 64: 541–565.
- Eigen M, Biebricher C (1988) Sequence Space and Quasispecies Distribution. In: Domingo E, Holland J, Ahlquist P, editors. *RNA Genetics*. Boca Raton: CRC Press. 211–245.
- ATCC NIH/3T3 ATCC CRL-11658.
- Yamayoshi S, Yamashita Y, Li J, Hanagata N, Minowa T, et al. (2009) Scavenger receptor B2 is a cellular receptor for enterovirus 71. *Nat Med* 15: 798–801.
- Yamayoshi S, Ohka S, Fujii K, Koike S (2013) Functional comparison of SCARB2 and PSGL1 as receptors for enterovirus 71. *J Virol* 87: 3335–3347.
- Yamayoshi S, Koike S (2011) Identification of a human SCARB2 region that is important for enterovirus 71 binding and infection. *J Virol* 85: 4937–4946.
- Zaini Z, Phuektes P, McMinn P (2012) Mouse adaptation of a sub-genogroup B5 strain of human enterovirus 71 is associated with a novel lysine to glutamic acid substitution at position 244 in protein VP1. *Virus Res* 167: 86–96.

Author Contributions

Conceived and designed the experiments: CBLV KBC. Performed the experiments: CBLV YX. Analyzed the data: CBLV KBC. Contributed reagents/materials/analysis tools: YX QN VTC KBC. Wrote the paper: CBLV KBC. Manuscript review/revision: VTC. Maintained some cell lines: QN YX. Provided the statistical analysis software: YX.

51. Arita M, Ami Y, Wakita T, Shimizu H (2008) Cooperative effect of the attenuation determinants derived from poliovirus sabin 1 strain is essential for attenuation of enterovirus 71 in the NOD/SCID mouse infection model. *J Virol* 82: 1787–1797.
52. Zaini Z, McMinn P (2012) A single mutation in capsid protein VP1 (Q145E) of a genogroup C4 strain of human enterovirus 71 generates a mouse-virulent phenotype. *J Gen Virol* 93: 1935–1940.
53. Liu CC, Chou AH, Lien SP, Lin HY, Liu SJ, et al. (2011) Identification and characterization of a cross-neutralization epitope of Enterovirus 71. *Vaccine* 29: 4362–4372.
54. Zaini Z, Phuektes P, McMinn P (2012) A reverse genetic study of the adaptation of human enterovirus 71 to growth in Chinese hamster ovary cell cultures. *Virus Res* 165: 151–156.
55. Miyamura K, Nishimura Y, Abo M, Wakita T, Shimizu H (2011) Adaptive mutations in the genomes of enterovirus 71 strains following infection of mouse cells expressing human P-selectin glycoprotein ligand-1. *J Gen Virol* 92: 287–291.
56. Lin JY, Chen TC, Weng KF, Chang SC, Chen LL, et al. (2009) Viral and host proteins involved in picornavirus life cycle. *J Biomed Sci* 16: 103.
57. Eigen M (1993) The origin of genetic information: viruses as models. *Gene* 135: 37–47.
58. Domingo E, Sheldon J, Perales C (2012) Viral quasispecies evolution. *Microbiol Mol Biol Rev* 76: 159–216.
59. Domingo E, Menéndez-Arias L, Holland JJ (1997) RNA virus fitness. *Rev Med Virol* 7: 87–96.
60. Domingo E (2002) Quasispecies theory in virology. *Journal of Virology* 76: 463–465.
61. Reed L, Muench H (1938) A simple method of estimating fifty per cent endpoints. *The American Journal of Hygiene* 27: 493–497.
62. Lindenbach BD, Evans MJ, Syder AJ, Wölk B, Tellinghuisen TL, et al. (2005) Complete replication of hepatitis C virus in cell culture. *Science* 309: 623–626.
63. Hall T (1999) BioEdit: a user-friendly biological sequence alignment editor and analysis program for Windows 95/98/NT. *Nucleic Acids Symposium Series* 41: 95–98.
64. Arnold K, Bordoli L, Kopp J, Schwede T (2006) The SWISS-MODEL workspace: a web-based environment for protein structure homology modelling. *Bioinformatics* 22: 195–201.
65. Guex N, Peitsch MC (1997) SWISS-MODEL and the Swiss-PdbViewer: an environment for comparative protein modeling. *Electrophoresis* 18: 2714–2723.